

Performance evaluation and optimization of a perovskite solar cell-thermoelectric generator hybrid system

Tianjun Liao^{a,b}, Qijiao He^a, Qidong Xu^a, Yawen Dai^a, Chun Cheng^a, Meng Ni^{a*}

^a *Department of Building and Real Estate, The Hong Kong Polytechnic University, Hung Hom, Kowloon, Hong Kong, China*

^b *Department of Physics and Energy, Chongqing University of Technology, Chongqing 400054, China*

Abstract: In order to improve the photo-to-electric energy conversion efficiency, a hybrid system is proposed by integrating a thermoelectric generator (TEG) with a perovskite solar cell (PSC). According to the derived formulas for the efficiency and power output of the hybrid system, three especial work states such as opened TEG, opened PSC, and PSC-TEG tandem cells are, respectively, discussed through numerical simulation. Further, we study the general work state, i.e., the PSC and the TEG independently drive their loads and are coupled with each other through energy balance equation. The matching loads $0.13\ \Omega$ and $12.3\ \Omega$ of the two subsystems and the optimum area $0.0324\ \text{m}^2$ of the PSC can be chosen to obtain the maximum efficiency 0.216. Moreover, the perovskite layer's optimum thickness $449.7\ \text{nm}$ is designed to obtain the overall maximum efficiency 0.229. For comparison, the hybrid system achieves improved overall energy efficiency by harnessing the waste heat produced in the PSC. The proposed model may provide some theoretical bases for the optimal design of practical PSC–TEG hybrid systems.

Key words: perovskite solar cell (PSC); thermoelectric generator (TEG); hybrid system; performance evaluation; matching load

*Corresponding author (M. Ni)

Email: meng.ni@polyu.edu.hk; Tel: 852-27664152; Fax: 852-27645131

<p>Nomenclature</p> <p>A area (m^2)</p> <p>c speed of light ($\text{m} \cdot \text{s}^{-1}$)</p> <p>$d$ thickness (nm)</p> <p>E photon energy (eV)</p> <p>E_g PV cell bandgap (eV)</p> <p>G solar irradiance ($\text{W} \cdot \text{cm}^{-2}$)</p> <p>$q$ elementary positive charge (C)</p> <p>h Planck constant ($\text{eV} \cdot \text{s}$)</p> <p>I electrical current (A)</p> <p>J_{PV} output current density of PSC ($\text{A} \cdot \text{m}^{-2}$)</p> <p>$J_{\text{ph}}$ photocurrent density ($\text{A} \cdot \text{m}^{-2}$)</p> <p>$J_0$ reverse saturation current density ($\text{A} \cdot \text{m}^{-2}$)</p> <p>$j$ dimensionless current of the TEG</p> <p>k_B Boltzmann constant ($\text{J} \cdot \text{K}^{-1}$)</p> <p>$K$ heat transfer coefficient ($\text{W} \cdot \text{K}^{-1}$)</p> <p>$l$ length (cm)</p> <p>n number of p-n couple</p> <p>P power output (W)</p> <p>Q heat flow (W)</p> <p>R_s series internal resistance ($\Omega \cdot \text{m}^2$)</p> <p>R_{sh} shunt resistance ($\Omega \cdot \text{cm}^2$)</p> <p>R_{TE} internal resistance of TEG ($\Omega \cdot \text{m}^2$)</p> <p>R internal resistance of TEG (Ω)</p> <p>R_{L1} load resistance of PSC (Ω)</p> <p>R_{L2} load resistance of TEG (Ω)</p> <p>S spectral irradiation intensity ($\text{W} \cdot \text{m}^{-2} \cdot \text{nm}^{-1}$)</p> <p>$T$ temperature (K)</p> <p>U heat transfer coefficient per area ($\text{W} \cdot \text{m}^{-2} \cdot \text{K}^{-1}$)</p> <p>$V$ voltage (V)</p> <p>v wind velocity ($\text{m} \cdot \text{s}^{-1}$)</p> <p>$Z$ figure of merit of the TEG materials (K^{-1})</p>	<p><i>Greek symbols</i></p> <p>α Seebeck coefficient ($\text{V} \cdot \text{K}^{-1}$)</p> <p>$\rho$ electrical resistivity ($\Omega \cdot \text{m}$)</p> <p>κ thermal conductivity ($\text{W} \cdot \text{K}^{-1} \cdot \text{m}^{-1}$)</p> <p>$\varepsilon$ electromotive force (V)</p> <p>λ wavelength of sunlight (m)</p> <p>γ structure parameter (m)</p> <p>η efficiency</p> <p>η_{M} overall maximum efficiency</p> <p><i>Subscript</i></p> <p>avg average</p> <p>amb ambient</p> <p>opt optimum</p> <p>OC open-circuit</p> <p>SC short-circuit</p> <p>p p type semiconductor</p> <p>PV photovoltaic</p> <p>TE thermoelectric</p> <p>H hot side</p> <p>L cold side</p> <p>n n type semiconductor</p> <p>max maximum</p> <p>min minimum</p> <p>M overall efficiency</p> <p><i>Abbreviations</i></p> <p>ETL electron transport layer</p> <p>HTL hole transport layer</p> <p>IPCE incident photon-to-electron conversion efficiency</p> <p>OCV open-circuit voltage</p> <p>PSC perovskite solar cell</p> <p>PCBM phenyl-C61-butyric acid methyl ester</p> <p>PEDOT: PSS poly (3, 4-ethylenedioxythiophene) polystyrene sulfonate</p> <p>TEG thermoelectric generator</p>
--	--

1. Introduction

As an important form of solar energy utilization, photovoltaic (PV) power generation directly converts solar energy into electricity. However, the current photo-to-electric energy conversion efficiency of the PV cells is still low due to that only energy of the sup-band-gap photons can be partly converted into electricity, while the energy of sub-band-gap photons are fully converted into thermal losses [1]. The irreversible thermal loss causes the PV cells to operate at high temperature state and present small efficiency. Consequently, improving the efficiency of the PV cells is a key issue. Coupling thermoelectric generators (TEGs) with PV cell is an important method to improve the solar energy utilization of the PV cell [2-8]. Xuan's group attempted to enhance the performance of PV-TE hybrid systems through photon management [2], concentrated spectrum split [3], and optimal design of thermal concentration ratio [4]. Li *et al.* [5] improved the efficiency and experimentally verified the feasibility of a novel PV-TE hybrid system by means of micro-channel heat pipe array. The comparison between the hybrid system and the pure PV were made. The tested results show that the efficiency of novel system can achieve 14% as the PV temperatures are about 20 °C higher than the ambient temperature. Feng *et al.* [6] established a one-dimensional steady-state heat conduction model of a PV-TE coupled system and studied the performance under different conditions of PV cell efficiency temperature coefficient and thermoelectric figure of merit. It is found that the coupled system has a relatively high efficiency when the thermal diffusion factor of the condenser system is around 3.0. Under the low-concentrated and natural light conditions, the parametric optimal design problem and the matching loads of two PV-TE hybrid systems were studied in our works [7, 8].

Apart from the commercial silicon-based PV cell, organic–inorganic hybrid halide perovskites material, such as $\text{CH}_3\text{NH}_3\text{PbI}_3$, have shown great promise as new absorber materials for low-cost highly efficient perovskite solar cells (PSCs) that have generated significant interest among the scientific and photovoltaic community due to excellent optical, electrical properties and ease of fabrication [9]. Similarly, the irreversible thermal losses are also produced in the PSC and directly released into ambient, which impact the efficiency and the lifetime of the PSC. Some newly published works are focusing on further improving the efficiency by integrating TEG with PSC. Xu *et al.* [10] proposed a hybrid device by integrating the hole-conductor-free PSC based on $\text{TiO}_2/\text{ZrO}_2/\text{carbon}$ structure and the TEG. The TEG generates additional electricity to improve the system efficiency by converting the thermal energy into electricity through the Seebeck effect. An optimized state is obtained with a maximum efficiency of 20.3% and open-circuit voltage (OCV) of 1.29 V under the condition of AM 1.5 G. Fu *et al.* [11] integrated a PSC with a TEG to form a hybrid system that can convert solar energy into electricity by simultaneously utilizing the sunlight and the waste heat from the PSC. The series and parallel connecting modes of subcells for the match with the same-size TEG were studied. The results showed that with the combination of series and parallel connected modes of the PSC subcells, the key parameters were adjusted to obtained a peak efficiency of 12.7% with an OCV of 6.80 V and a maximum power output of 103 mW under the condition of AM 1.5 G. Zhou *et al.* [12] demonstrated an efficient PSC-TEG hybrid system with four-terminal configuration. The bandgap of top PSC is turned to ultimately realize high solar energy conversion efficiency. Using perovskite with a composition of $\text{CH}_3\text{NH}_3\text{Pb}(\text{I}_{0.95}\text{Br}_{0.05})_3$ (bandgap: 1.61 eV), a state-of-the-art efficiency of

over 23% can be achieved. This work proves that the low-grade heat from PSCs can be recovered and utilized by TEG, and provides a promising route to improve the utilization of solar radiation based on PSCs. Liu *et al.* [13] proposed a novel integration of carbon counter electrodes-based PSCs and TEGs. The hybrid system exhibits obvious enhancement: the overall conversion efficiency increases from 9.88% to 12.6% after integration. The work opens up new avenues for the realization of high-performance, wide sunlight-harvesting PSC-TEG hybrid systems. Zhang *et al.* [14] demonstrated the feasibility of the PSC-TEG hybrid system due to the PSC with low temperature coefficient. Compared to the single PSC's efficiency 17.8%, the efficiency of the coupled system can be improved to 18.6%. The influences of thermal concentration on the design cost and the performance of the hybrid system were discussed.

Despite a growing literature on this topic, the reported works are mainly focused on the thermal and electrical characteristics of the PSC-TEG tandem cells, of which the hot side's temperature is directly given or tested. Nevertheless, there are still some unsolved problems. The energy balance equation between the two subsystems has not been established to determine the hot side's temperature of the hybrid system that is operated at three special work states such as opened TEG, opened PSC, and PSC-TEG tandem cells. What's more, there is no global optimization of parameters on the PSC-TEG hybrid system such as thermal parameter (e.g. the perovskite layer's temperature), the electrical parameters of the two subsystems (e.g. the voltage, current, and loads), and the structure parameters (e.g. the perovskite layer's thickness and area) of the PSC. In the present work, the PSC-TEG hybrid system is further investigated. Analytical expressions for the efficiency and power output of

the hybrid system are derived. The operating temperature of the PSC is numerically calculated by solving the energy balance equation. Special operating states such as opened TEG, opened PSC, and PSC-TEG tandem cells are, respectively, discussed. Further, the state that the PSC and the TEG independently drive their loads is investigated to improve efficiency of the hybrid system by analyzing and optimizing various device parameters.

2. Model description of a PSC–TEG hybrid system

The schematic diagram of a PSC-TEG hybrid system and two equivalent circuits of the PSC and TEG are shown in Fig. 1. In the combined system, PSC and TEG are electrically isolated but thermally connected. In this hybrid system, the thermal energy from the PSC can be well utilized to improve the photo-to-electricity energy conversion efficiency. The PV system consists of the PSC with thickness d , back electrode, indium tin oxide (ITO), glass, hole transport layer (HTL) and electron transport layer (ETL). The HTL and ETL are, respectively, made of PEDOT: PSS [poly (3, 4-ethylenedioxythiophene) polystyrene sulfonate] and PCBM (phenyl-C61-butyric acid methyl ester) responsible for transporting the electrons and holes to respective electrodes for efficient extraction [15]. Light is absorbed in the perovskite layer which gives rise to free electrons and holes [16]. These free charge carriers then diffuse and drift under the influence of the electric field, with electrons moving toward the ETL and holes toward the HTL. The hot side of the TEG is attached to the bottom of the PSC by the conduction material, the temperature at the hot side of the TEG is assumed to equal to that of the PSC, i.e., $T_H = T_{PV}$. The shunt resistance R_{sh} and the series internal resistance R_s of the PSC are $1.2\Omega \cdot m^2$ and $9 \times 10^{-4} \Omega \cdot m^2$ [17]. The PSC driven by the sunlight can generate the photocurrent density J_{ph} , the reverse saturation current density J_0 ,

and the output density J_{PV} . The current J_{PV} go through the load resistance R_{L1} can generate electrical power [18]. The TEG with internal resistance R is based on the Bi_2Te_3 materials due to its high-performance at small temperature difference [19, 20]. The TEG operated at two different temperatures T_H and T_L can generate the voltage V_{TE} and the electrical current I_{TE} based on the Seebeck effect. The electrical current I_{TE} go through the load resistance R_{L2} can generate electricity. The hot side and cold side of the TEG absorb and release heat flows Q_H and Q_L , respectively.

2.1. The power output of a PSC

An electrical circuit with a single diode is considered as the equivalent PSC in the present paper, as shown in Fig. 1(b). The current–voltage characteristics equation of a PSC is given by [12]:

$$J_{PV} = J_{ph} - J_0 \left\{ \exp \left[\frac{q(J_{PV}R_s + V_{PV})}{k_B T_{PV}} \right] - 1 \right\} - \frac{V_{PV} + J_{PV}R_s}{R_{sh}}, \quad (1)$$

where q is the charge of an electron. k_B is the Boltzmann constant.

The photocurrent density J_{ph} and reverse saturation current density J_0 at the operating-cell temperature and solar irradiance can be, respectively, expressed as [17, 21]

$$J_{ph} = q \int_0^{\lambda_g} \frac{\lambda}{hc} S(\lambda) IPCE(\lambda) d\lambda \quad (2)$$

and

$$J_0 = \frac{2\pi q}{h^2 c^3} \int_{E_g}^{\infty} \frac{E^2 dE}{\exp[E/(k_B T_{PV})] - 1}, \quad (3)$$

where $IPCE(\lambda)$ is the incident photon-to-electron conversion efficiency (IPCE). λ is the wavelength of the sunlight. $S(\lambda)$ denotes the spectral irradiation intensity of AM 1.5G. h is Planck's constant. c is speed of light. E is the photon energy. $E_g = hc/\lambda_g = 1.55 \text{ eV}$ is

the band-gap in the PSC. Based on the above equations, the power output generated in the PSC is expressed as

$$P_{PV} = V_{PV} J_{PV} A_{PV}, \quad (4)$$

where A_{PV} is the area of the PSC.

2.2. The power output of a TEG

The TEG is made of n- and p-type semiconductor elements that are connected electrically in series and thermally in parallel. It can directly convert thermal energy into output voltage according to the Seebeck effect. When it is operated under a temperature difference $(T_H - T_L)$ and connected to a load resistance R_{L2} , power output P_{TE} can be generated. The operating TEG includes three physics effects, such as the Newton cooling law, the Joule law, and the Peltier effect. The heat flows releasing from the PSC to the TEG Q_H , and flowing from the TEG to the environment, Q_L , yield [19, 20]

$$Q_H = \alpha T_H I_{TE} + K(T_H - T_L) - \frac{1}{2} I_{TE}^2 R \quad (5)$$

and

$$Q_L = \alpha T_L I_{TE} + K(T_H - T_L) + \frac{1}{2} I_{TE}^2 R, \quad (6)$$

where $\alpha = (\alpha_p - \alpha_n)n$, $K = (\kappa_p A_p / l_p + \kappa_n A_n / l_n)n$, and $R = (\rho_p l_p / A_p + \rho_n l_n / A_n)n$ are, respectively, the Seebeck coefficient, thermal conductivity, and electrical resistivity of the TEG. n is the number of p-n couple. l and A are the length and the cross-sectional area of the semiconductor element. ρ is the electrical resistivity and κ is the thermal conductivity of a TEG. The subscripts n and P designate n- and p-type elements. Commercial CP2-127-06 Melcor TEG is adopted in this work. The total Seebeck coefficient, resistivity, and thermal conductivity of a p-n couple can be computed by using equations as

[19]

$$\alpha_p - \alpha_n = (22224.0 + 930.6T_{\text{avg}} - 0.8805T_{\text{avg}}^2) \times 10^{-9}, \quad (7)$$

$$\rho_p + \rho_n = (5112 + 163.4T_{\text{avg}} + 0.6279T_{\text{avg}}^2) \times 10^{-10}, \quad (8)$$

and

$$\kappa_p + \kappa_n = (62605.0 - 277.7T_{\text{avg}} + 0.4131T_{\text{avg}}^2) \times 10^{-4}, \quad (9)$$

where $T_{\text{avg}} = (T_H + T_L)/2$ is the average temperature of the TEG. The area A_{TE} of the CP2-127-06 Melcor TEG is equal to $3.6 \times 10^{-3} \text{ m}^2$.

According to Eqs. (11) and (12), the power output P_{TE} of the TEG can be obtained as [7, 8]

$$P_{\text{TE}} = Q_H - Q_L = \alpha(T_H - T_L)I_{\text{TE}} - RI_{\text{TE}}^2 = R_{L2}I_{\text{TE}}^2. \quad (10)$$

The dependence of the operating current I_{TE} on the voltage V_{TE} is presented as [7, 8]

$$I_{\text{TE}} = \frac{V_{\text{TE}}}{R} = \frac{\alpha(T_H - T_L)}{R + R_{L2}}. \quad (11)$$

By using Eq (10), the power output P_{TE} generated in the TEG can be rewritten as [7, 8]

$$P_{\text{TE}} = \frac{ZK(T_H - T_L)^2}{(1 + R_{L2}/R)^2} \frac{R_{L2}}{R}, \quad (12)$$

It can be seen in Eq. 12, the power output and efficiency of the TEG are effected by the factors such as the resistance ratio R_{L2}/R , the figure of merit of the TEG materials Z , the temperatures T_H and T_L , and the thermal conductivity K of the TEG etc.

2.3. The power output and efficiency of the hybrid system

According to the energy balance analysis, the input heat flowing from the PSC to the TEG can be expressed as

$$Q_H = GA_{\text{PV}} - V_{\text{PV}}J_{\text{PV}}A_{\text{PV}}, \quad (13)$$

where G is the solar irradiance.

We assume the structure parameter of the TEG $A_p/l_p = A_n/l_n$. By using Eqs. (4), (5), and Eq. (13) can be rewritten as

$$\frac{Z(T_H - T_L)^2}{2(1 + R_{L2}/R)^2} - \left(\frac{ZT_H}{1 + R_{L2}/R} + 1 \right) (T_H - T_L) + \frac{\gamma(V_{PV}J_{PV} - G)}{\kappa_p + \kappa_n} = 0, \quad (14)$$

where $\gamma = A_{PV}/(nA_p/l_p)$ is a structure parameter. In the model description, it has been assumed $T_H = T_{PV}$. When the relevant parameters R_{L2}/R and V_{PV} and of PSC and TEG are given, T_{PV} and J_{PV} can be calculated by solving Eq. (1)-(14).

Using Eqs. (5) and (15), the power output P and the efficiency η of the hybrid system can be expressed as

$$P = P_{PV} + P_{TE} = V_{PV}J_{PV}A_{PV} + \frac{ZK(T_H - T_L)^2}{(1 + R_{L2}/R)^2} \frac{R_{L2}}{R} \quad (15)$$

and

$$\eta = \frac{P}{GA_{PV}} = \frac{V_{PV}J_{PV}}{G} + \frac{1}{GA_{PV}} \frac{ZK(T_H - T_L)^2}{(1 + R_{L2}/R)^2} \frac{R_{L2}}{R}. \quad (16)$$

3. Performance evaluation

3.1 Performance evaluation of the single PSC

When the TEG circuit is opened, it doesn't generate electricity and only acts as a cooler (heat sink) of the PSC. In such a case, the thermal conductivity per unit area U is equal to K/A_{PV} . The open-circuit voltage $V_{TE,OC}$ is equal to $\alpha(T_H - T_L)$. By using Eqs. (4), (9), (14), and (16), the dependences of η_{PV} , T_{PV} , $V_{TE,OC}$, and U on V_{PV} is illustrated in Fig. 2, where $V_{PV,OC}$ is the open-circuit voltage of the PSC. In Fig. 2(a), the temperature T_{PV} firstly decreases and then increase with increase of V_{PV} , it can achieve a minimum temperature $T_{PV,min}$, where the efficiency η_{PV} of the PSC can archive its maximum value $\eta_{PV,max}$, and a

corresponding value $V_{PV,opt}$ can be obtained. Fig. 2(a) shows that the temperature T_{PV} of the PSC under the condition of $V_{PV} = 0$ is equal to that of the PSC under condition of $V_{PV} = V_{PV,OC}$. In these two work conditions, the PSC only acts as a solar thermal collector. Figs. 2(a) and (b) indicate that the open-circuit voltage $V_{TE,OC}$ is determined by the temperature T_{PV} , one can obtain a minimum value of $V_{TE,OC}$ of as $T_{PV} = T_{PV,min}$, because the temperature T_H on hot side of the TEG depends on V_{PV} , manuscript varies with the variation of according to Eq. (9). Although U depends on T_{PV} , one can find that U is approximately equal to $40 \text{ W} \cdot \text{K}^{-1} \cdot \text{m}^{-2}$, which is larger than the natural convection thermal conductivity per unit area $5 \text{ W} \cdot \text{K}^{-1} \cdot \text{m}^{-2}$. Consequently, the opened TEG also can improve the performance of the PSC, because the temperature of the PSC is lower than that of the pure PSC. However, In other words, when special cooling methods are used for the single PSC, the heat transfer coefficient between the single PSC and the ambient will be raised, causing that the performance of the single PSC is better than that of the hybrid system without special cooling treatment.

3.2 Performance evaluation of the single TEG

When the PSC circuit is opened, it doesn't generate electricity and only acts as a solar thermal collector to drive the TEG. In such a case, the energy conversion efficiency of the TEG is equal to η_{TE} . By using Eqs. (12), (14), and (16), the dependences of η_{TE} and T_H on R_{L2}/R is depicted in Fig. 3. It is observed from Fig. 3 that T_H is a monotonically increasing function of R_{L2}/R , whereas η_{TE} is not a monotonic function of R_{L2}/R , one can obtain a maximum efficiency $\eta_{TE,max}$ and the corresponding values $(R_{L2}/R)_{opt}$ and $T_{H,opt}$. The internal resistance R of the TEG can be calculated by using Eqs. (8) and (14). Due to

the internal irreversible losses of the TEG, the result $(R_{L2}/R)_{\text{opt}} > 1$ is occurred. The power output P_{TE} generated in the TEG increases as R_{L2}/R is increased due to the increase of the temperature T_{H} , and consequently, the R_{L2}/R should be situated in the region of $R_{L2}/R > (R_{L2}/R)_{\text{opt}}$. Making a comparison between the Fig. 2(a) and Fig. 3(a), one can find that the performance of the single PSC system is better than that of the single TEG system. Fig. 3(b) shows that the open-circuit voltage $V_{\text{PV,OC}}$ of the PSC monotonically decreases of the R_{L2}/R , this phenomenon is determined by the Eqs. (1) and (14). Inserting $J_{\text{PV}} = 0$ into Eq. (1) and integrating Eq. (14), the variation of $V_{\text{PV,OC}}$ with R_{L2}/R can be obtained.

3.3 Performance evaluation of the PSC-TEG tandem cells

When the two circuits of the TEG and PSC are connected in series, the equivalent circuit is simplified to Fig. 4(a). The current–voltage characteristics equation is rewritten as [12]:

$$J = J_{\text{ph}} - J_0 \left\{ \exp \left[\frac{q(V + J(R_{\text{s}} + R_{\text{TE}}) - \varepsilon_{\text{TE}})}{k_{\text{B}} T_{\text{PV}}} \right] - 1 \right\} - \frac{V + J(R_{\text{s}} + R_{\text{TE}}) - \varepsilon_{\text{TE}}}{R_{\text{sh}}}, \quad (17)$$

where V is total output voltage. The TEG's electromotive force $\varepsilon_{\text{TE}} = \alpha(T_{\text{H}} - T_{\text{L}})$ is generated based on the Seebeck effect. As the system is operated at steady state, the equilibrium equation in Ref. [12] can be simplified to Eq. (14) in present work. Like the previous works [10-13], the current–voltage characteristics of the tandem cells depend on those of the PSC, as verified in Fig. 4(b). The performance comparisons are described in Table 1. Fig. 4(c) shows that the temperature T_{PV} and the efficiency η of the tandem cells is not a monotonic function of V , and thus, one can obtain a maximum efficiency a η_{max} and the corresponding values V_{opt} and $T_{\text{PV,opt}}$. Making comparisons between the Fig. 4(c) and Figs. 2(a) and 3(a), one can find that the performance of the tandem cells is better than the single TEG system and the single PSC system. As the pure PSC is operated at

environment, it can reach 54 °C due to the strong absorptivity and photo-thermal conversion [10, 11]. The operating temperature can be approximately expressed as [22]:

$$T_{PV} \approx T_{amb} + \frac{G}{a + bv}, \quad (18)$$

where v is the wind velocity. $a = 25.5 \text{ W} \cdot ^\circ\text{C}^{-1} \cdot \text{m}^{-2}$ is the coefficient describing the effect of the radiation on the module temperature. $b = 10.5 \text{ W} \cdot \text{s} \cdot ^\circ\text{C}^{-1} \cdot \text{m}^{-3}$ describes the cooling by the wind. As $v = 0.2 \text{ m} \cdot \text{s}^{-1}$ is chosen, the temperature $T_{PV} \approx 336 \text{ K}$ can be obtained. It can be found in Table 1 that all the temperatures of the PSCs in the tandem cells are lower the temperature of the pure PSC. The results indicate that the PSC's temperature can be cooled by means of the TEG. Compared to the single PSC, the improvement of voltage is achieved in the tandem cells. However, the disadvantage of the tandem cells is that the electric currents of the two sub-cells should be matched. The electrical losses may be generated.

3.4 Performance evaluation and optimization of the hybrid system

In Fig. 5(a), the variations of the temperature T_{PV} with V_{PV} and R_{L2}/R have been revealed in the above discussion. The volt-ampere characteristic equation of the PSC leads that J_{PV} monotonically decreases with increase of V_{PV} , as shown in Fig. 5(b). Eq. (1), there exists negative correlation between J_{PV} and T_{PV} . Because of the variation of the temperature T_{PV} with R_{L2}/R and the negative correlation between J_{PV} and T_{PV} , J_{PV} monotonically decreases with increase of R_{L2}/R , as verified in Fig. 5(b). Fig. 5(c) shows that the dimensionless current j changes negligibly with V_{PV} , while monotonically decreases as R_{L2}/R is increased. Fig. 5(c) displays that the dimensionless current j is a monotonically decreasing function of R_{L2}/R as V_{PV} is fixed, changes negligibly with V_{PV} for a given R_{L2}/R . Fig. 5(d) reveals that there exist optimal values $(R_{L2}/R)_{opt}$ and $V_{PV,opt}$ at which the

efficiency attains its optimal value η_{opt} . By using $(R_{L2}/R)_{\text{opt}}$ and $V_{\text{PV,opt}}$, the optimal values $T_{\text{PV,opt}}$, $J_{\text{PV,opt}}$, and j_{opt} can be calculated. Thus, the optimal performance of the hybrid system can be achieved by choosing reasonable values of system parameters. It is worth to note that the parametric optimal values vary with A_{PV} . In next section, the effects of A_{PV} on the optimal performances of the hybrid system will be discussed.

Fig. 6 shows clearly that one can obtain a maximum efficiency η_{max} and the relevant optimum values $A_{\text{PV},\eta}$, $T_{\text{PV},\eta}$, $V_{\text{PV},\eta}$, $J_{\text{PV},\eta}$, $(R_{L2}/R)_{\eta}$, and j_{η} . The analysis is as follows. Fig. 6(a) shows that as the sunlight absorption area A_{PV} is very small, the hot side temperature of the TEG isn't efficiently improved, and thus, the power generation is small. As A_{PV} is very large, although the TEG can be efficiently driven by the PSC, while the high operating temperature T_{PV} decreases the PSC's electricity generation, and thus, the total efficiency of the hybrid system is still small. This indicates that an optimum structure parameter $A_{\text{PV},\eta}$ is preferred for the design of the PSC-TEG hybrid system. The power output P_{max} is at the maximum efficiency η_{max} can be expressed as

$$P_{\text{max}} = (GA_{\text{PV},\eta})\eta_{\text{max}}. \quad (19)$$

Additionally, the increase of $T_{\text{PV,opt}}$ leads to the results that the energy balance Eq. (14) should be satisfied by increasing j_{opt} and decreasing $V_{\text{PV,opt}}$, $J_{\text{PV,opt}}$, and $(R_{L2}/R)_{\text{opt}}$. By using $A_{\text{PV},\eta} = 3.24 \times 10^{-2} \text{ m}^2$, $J_{\text{PV},\eta} = 207 \text{ A} \cdot \text{m}^{-2}$, $V_{\text{PV},\eta} = 0.856 \text{ V}$, $(R_{L2}/R)_{\eta} = 1.34$, and Eq. (8), the matching load resistances $R_{L1,\eta} = 0.13 \Omega$ and $R_{L2,\eta} = 12.3 \Omega$ can be determined. From analyses above, the performance of the hybrid system can achieve the optimum by choosing reasonable values of R_{L1} and R_{L2} . The numerical results of the optimal load resistance will supply a theoretical basis for the optimal operation of the PSC-TEG hybrid

system.

Obviously, η_{\max} is an important parameter, because it determines an upper bound for the efficiency of the hybrid system. The dependences the maximum efficiency η_{\max} and the photo-generation current density J_{ph} on perovskite layer thickness d , as described in Fig 7. The photo-generation current density J_{ph} as a function of d is based on Ref. [17]. Fig. 7 shows that the variations of η_{\max} with d is similar with that of J_{ph} with d .

When perovskite layer thickness d photo-generation current density J_{ph} are, respectively, equal to d_{M} and J_{M} , η_{\max} attains its maximum value $\eta_{\text{M}} = 0.229$. Making comparisons between Fig. 7 and Figs. 2, 3, and 4, one can find that the maximum efficiency of the PSC-TEG is better than that of the single PSC, single TEG, and tandem cells. The maximum efficiency of the present hybrid system is 1.24 times than that of the pure PSC in Ref. [17]. The results reveal that the energy cascade utilization system can decrease thermal loss and improve efficiency. However, the disadvantage of this system is that the PSC operates at high temperature, of which the lifetime may be limited.

4. Conclusions

We have established a theoretical model of the PSC-TEG hybrid system. The main research results are listed as follows:

(1) The performances of the three especial work states such as single PSC, single TEG, and PSC-TEG tandem cells are investigated and compared. As the opened TEG works as a heat sink, the maximum efficiency of the single PSC 0.204 can be achieved. As the opened PSC works as a solar collector, the maximum efficiency of the single TEG 0.0516 can be presented. In addition, the maximum efficiency 0.208 of the PSC-TEG tandem cells can be

obtained.

(2) The performance evaluation PSC and TEG independent work state are numerically studied. The maximum efficiency $\eta_{\max}=0.216$ and the corresponding optimum conditions $A_{\text{PV},\eta}=3.24\times 10^{-2}\text{ m}^2$, $J_{\text{PV},\eta}=207\text{ A}\cdot\text{m}^{-2}$, $V_{\text{PV},\eta}=0.856\text{ V}$, $(R_{\text{L2}}/R)_{\eta}=1.34$, $R_{\text{L1},\eta}=0.13\ \Omega$, and $R_{\text{L2},\eta}=12.3\ \Omega$ are obtained.

(3) The overall maximum efficiency $\eta_{\text{M}}=0.229$ and the perovskite layer's optimum thickness $d_{\text{M}}=449.7\text{ nm}$ are obtained. Comparing with the single PSC system, the PSC-TEG hybrid system has advantages of increasing the power output, improving of the conversion efficiency of solar energy, and reducing emission of lower quality waste heat.

The results obtained here will provide opens up new avenues for the optimal design of real hybrid systems. In the future, the performances of the hybrid system can be further enhanced by optimizing the structure of the PSC [23] and selecting the high figure of merit of the TEG materials [24, 25].

Acknowledgements

This work has been supported by the Science and Technology Research Program of Chongqing Municipal Education Commission (Grant No. KJQN201901144) and Scientific Research Foundation of Chongqing University of Technology (Grant No. 2019ZD22), People's Republic of China. M. NI also thanks the financial support by Hong Kong Polytechnic University (Project ID: P0014036, account: G-YW3T).

References

- [1] Y. Zhang, Y. Xuan, Preparation of structured surfaces for full-spectrum photon management in photovoltaic-thermoelectric systems, *Sol. Energy Mater. Sol. Cells* 2017; 169: 47–55.
- [2] Y. Zhang, Y. Xuan, Biomimetic omnidirectional broadband structured surface for photon management in photovoltaic–thermoelectric hybrid systems, *Sol. Energy Mater. Sol. Cells* 2016; 144: 68–77.
- [3] E. Yin, Q. Li, Y. Xuan. A novel optimal design method for concentration spectrum splitting photovoltaic–thermoelectric hybrid system. *Energy* 2018; 163: 519-532.
- [4] E. Yin, Q. Li, Y. Xuan. One-day performance evaluation of photovoltaic-thermoelectric hybrid system. *Energy*, 2018; 143: 337-346.
- [5] G. Li, S. Shittu, X. Zhao, X. Ma. Preliminary experiment on a novel photovoltaic-thermoelectric system in summer. *Energy* 2019; 188: 116041.
- [6] L. J. Feng, E. S. Yin, Q. Li, Optimization of the photovoltaic-thermoelectric hybrid system with and without optical concentrator. *Chin. Sci. Bull.* 2019; 64: 1943–1952.
- [7] T. Liao, B. Lin, Z. Yang Performance characteristics of a low concentrated photovoltaic-thermoelectric hybrid power generation device. *Int. J. Therm. Sci.*, 2014; 77: 158–164.
- [8] J. Lin, T. Liao, B. Lin, Performance analysis and load matching of a photovoltaic–thermoelectric hybrid system, *Energy Convers, Manage* 2015; 105: 891–899.
- [9] M. Grätzel, The light and shade of perovskite solar cells, *Nat. Mater.* 2014; 13: 838–842.
- [10] L. Xu, Y. Xiong, A. Mei, Y. Hu, Y. Rong, Y. Zhou, B. Hu, and H. Han. Efficient Perovskite Photovoltaic-Thermoelectric Hybrid Device. *Advanced Energy Materials* 2018, 8: 1702937.
- [11] P. Fu, W. Qin, S. Bai, D. Yang, L. Chen, X. Guo, C. Li, Integrating large-area perovskite solar module with thermoelectric generator for enhanced and stable power output. *Nano Energy* 2019; 65: 104009.
- [12] Y. Zhou, X. Yin, Q. Zhang, N. Wang, A. Yamamoto, K. Koumoto, H. Shen, H. Lin. Perovskite solar cell-thermoelectric tandem system with a high efficiency of over 23%.

Materials Today Energy 2019, 12: 363–370.

[13] Z. Liu, B. Sun, Y. Zhong, X. Liu, J. Han, T. Shi, Z. Tang, G. Liao, Novel integration of carbon counter electrode based perovskite solar cell with thermoelectric generator for efficient solar energy conversion. Nano Energy 2017; 38: 457–466.

[14] J. Zhang, Y. Xuan, L. Yang, A novel choice for the photovoltaic–thermoelectric hybrid system: the perovskite solar cell, Int. J. Energy Res. 2016; 40: 1400–1409.

[15] S. Wahid, M. Islam, Md. S. S. Rahman, Md. K. Alam. Transfer Matrix Formalism-Based Analytical Modeling and Performance Evaluation of Perovskite Solar Cells. IEEE Transac. Electron Devices 2017; 64 : 5034–5041.

[16] X. Sun, R. Asadpour, W. Nie, A. D. Mohite, M. A. Alam. A physics-based analytical model for perovskite solar cells. IEEE J. Photovoltaics 2015; 5: 1389–1394.

[17] L. Zhang, S. Ding, G. Qin. Efficiency simulations on perovskite solar cells only using experimentally determined reflectance and transmittance data. Sol. Energy Mater. Sol. Cells 2019; 201: 110039.

[18] G. A. Nemnes, C. Besleaga, A. G. Tomulescu, I. Pintilie, L. Pintilie, K. Torfason, A. Manolescu. Dynamic electrical behavior of halide perovskite based solar cells. Sol. Energy Mater. Sol. Cells 2017; 159: 197–203.

[19] S. B. Riffat, X. Ma, R. Wilson. Performance simulation and experimental testing of a novel thermoelectric heat pump system. Appl. Thermal. Eng. 2006; 26: 494.

[20] S. Su, T. Liu, Y. Wang, X. Chen, J. Wang, J. Chen. Performance optimization analyses and parametric design criteria of a dye-sensitized solar cell thermoelectric hybrid device. Appl. Energy 2014; 120: 16.

[21] K. Seki. Equivalent circuit representation of hysteresis in solar cells that considers interface charge accumulation: Potential cause of hysteresis in perovskite solar cells. Appl. Phys. Lett. 2016; 109: 033905.

[22] W. Tress, K. Domanski, B. Carlsen, A. Agarwalla, E.A. Alharbi, M. Graetzel, A. Hagfeldt. Performance of perovskite solar cells under simulated temperature-illumination real-world operating conditions Nat. Energy 2019, 4(7): 568–574.

[23] W.E.I. Sha, X. Ren, L. Chen, W.C.H. Choy. The efficiency limit of $\text{CH}_3\text{NH}_3\text{PbI}_3$ perovskite solar cells, Appl. Phys. Lett. 2015; 106: 221104.

- [24] H. Zhu, J. Mao, Z. Feng, J. Sun, Q. Zhu, Z. Liu, D. J. Singh, Y. Wang, Z. Ren. Understanding the asymmetrical thermoelectric performance for discovering promising thermoelectric materials. *Sci. Adv.* 2019; 5: eaav5813.
- [25] F. Zabihi, M. Tebyetekerwa, Z. Xu, A. Ali, A. K. Kumi, H. Zhang, R. Jose, S. Ramakrishna, S. Yang. Perovskite solar cell-hybrid devices: thermoelectrically, electrochemically, and piezoelectrically connected power packs. *J. Mater. Chem. A*, 2019; 7: 26661–26692.

List of Figures and Table

Fig. 1. (a) the schematic diagram of a PSC-TEG hybrid system, (b) the equivalent circuit of a PSC, and the (c) equivalent circuit of a TEG.

Fig. 2. The curves of (a) the efficiency η_{PV} and temperature T_{PV} of the PSC and (b) the open-circuit voltage $V_{TE,OC} = \alpha(T_H - T_L)$ and the thermal conductivity per unit area $U = K/A_{PV}$ of the TEG varying with the output voltage V_{PV} , where the parameters $G = 1000 \text{ Wm}^{-2}$, $T_L = 300 \text{ K}$, $d = 200 \text{ nm}$, $A_{PV} = 0.03 \text{ m}^2$, and $A_p/l_p = 4 \times 10^{-4} \text{ m}$ are chosen.

Fig. 3. The curves of (a) the efficiency η_{TE} and temperature T_H of the TEG and (b) the open-circuit voltage $V_{PV,OC}$ of the PSC varying with R_{L2}/R , where the values of the parameters are same as Fig. 2.

Fig. 4. (a) The equivalent circuit of the PSC-TEG tandem cells [10, 11], (b) the voltage-current characteristics curves of the PSC, the TEG, and the tandem cells, and (c) The curves of the efficiency η of the tandem cells and the temperature T_{PV} current as a function of the total output voltage V , where $A_p/l_p = A_n/l_n = 2.93 \times 10^{-3} \text{ m}$, $A_{PV} = A_{TE} = 3.6 \times 10^{-3} \text{ m}^2$, $R_{TE} = RA_{TE}$, and $n = 10$.

Fig. 5. The three-dimensional projection graphs of (a) the temperature T_{PV} of PSC, (b) the current density of J_{PV} the PSC, (c) the dimensionless current $j = \alpha I_{TE}/K$ of the TEG, and (d) the efficiency η of the hybrid system varying with variables V_{PV} and R_{L2}/R , where the values of the parameters are same as Fig. 2.

Fig. 6. (a) The optimal efficiency η_{opt} and PSC temperature $T_{PV,opt}$, (b) the optimal voltage $V_{PV,opt}$ and current density $J_{PV,opt}$ of the PSC, and (c) the optimal resistance ratio $(R_{L2}/R)_{opt}$ and dimensionless electric current j_{opt} of the TEG as a function of A_{PV} .

Fig. 7. The curves of the maximum efficiency η_{max} and the photo-current density J_{ph} as a function of d .

Table 1. The performance comparisons between the present work and Refs. [10-13], where $\Delta T = T_H - T_L$.

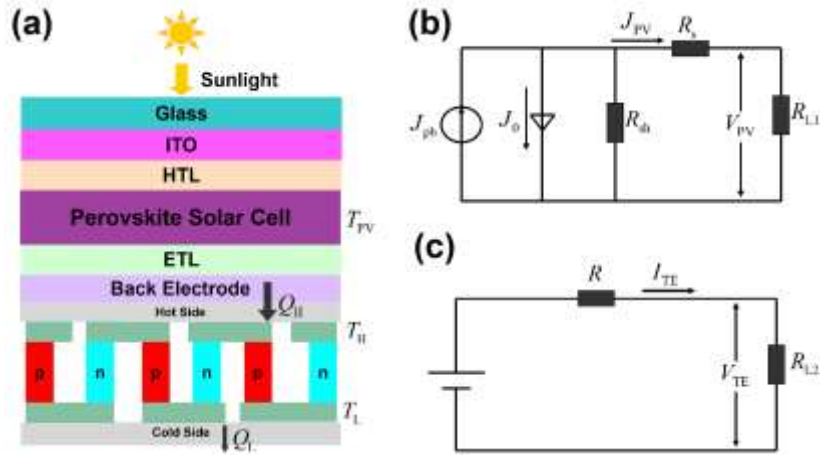


Fig. 1. (a) the schematic diagram of a PSC-TEG hybrid system, (b) the equivalent circuit of a PSC, and the (c) equivalent circuit of a TEG.

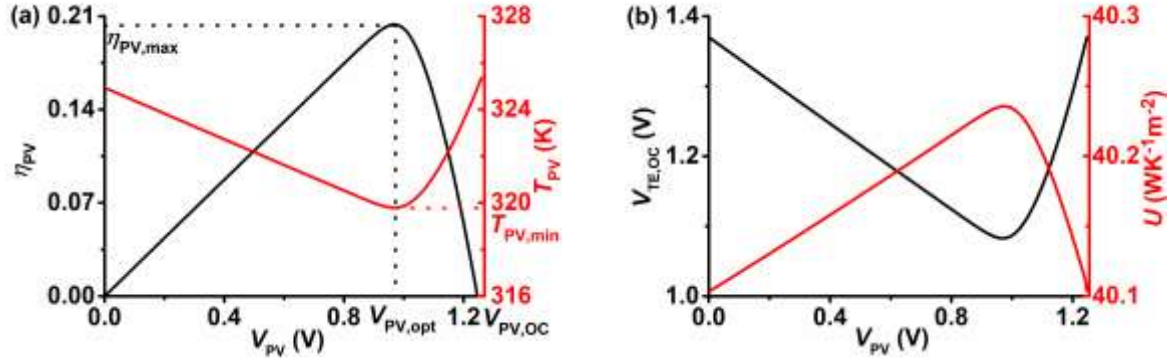


Fig. 2. The curves of (a) the efficiency η_{PV} and temperature T_{PV} of the PSC and (b) the open-circuit voltage $V_{TE,OC} = \alpha(T_H - T_L)$ and the thermal conductivity per unit area $U = K/A_{PV}$ of the TEG varying with the output voltage V_{PV} , where the parameters $G = 1000 W m^{-2}$, $T_L = 300 K$, $d = 200 nm$, $A_{PV} = 0.03 m^2$, and $A_p/l_p = 4 \times 10^{-4} m$ are chosen.

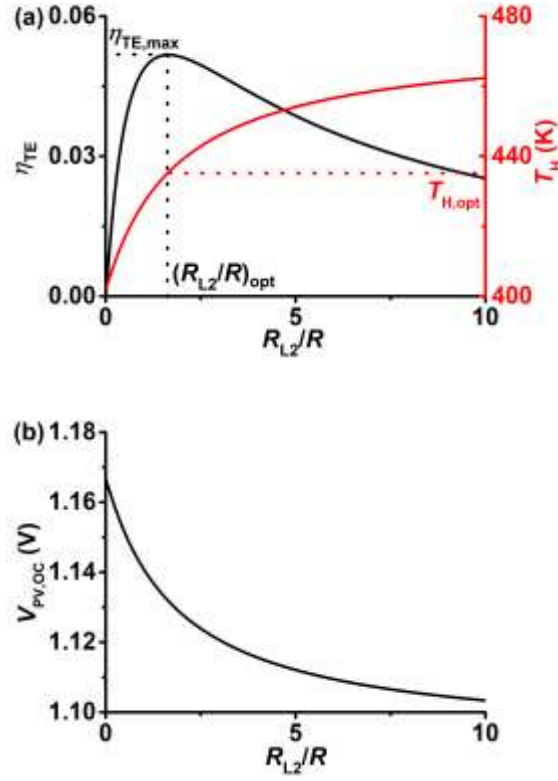


Fig. 3. The curves of (a) the efficiency η_{TE} and temperature T_H of the TEG and (b) the open-circuit voltage $V_{PV,OC}$ of the PSC varying with R_{L2}/R , where the values of the parameters are same as Fig. 2.

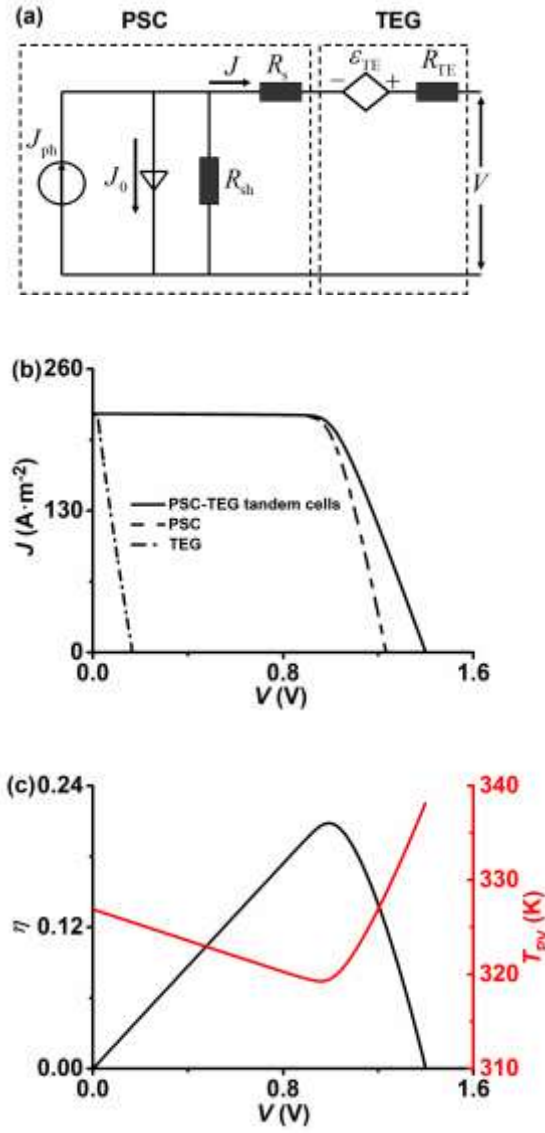


Fig. 4. (a) The equivalent circuit of the PSC-TEG tandem cells [10, 11], (b) the voltage-current characteristics curves of the PSC, the TEG, and the tandem cells, and (c) The curves of the efficiency η of the tandem cells and the temperature T_{PV} current as a function of the total output voltage V , where $A_p/l_p = A_n/l_n = 2.93 \times 10^{-3} \text{ m}$, $A_{PV} = A_{TE} = 3.6 \times 10^{-3} \text{ m}^2$, $R_{TE} = RA_{TE}$, and $n = 10$.

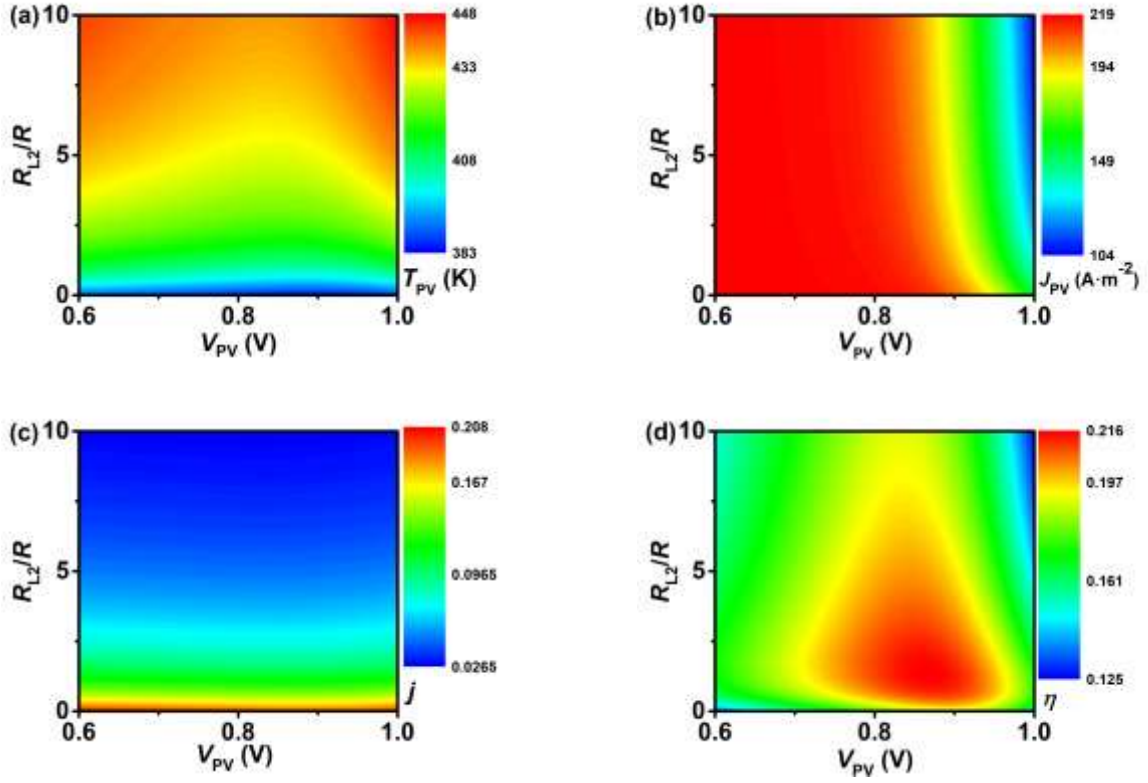


Fig. 5. The three-dimensional projection graphs of (a) the temperature T_{PV} of PSC, (b) the current density of J_{PV} the PSC, (c) the dimensionless current $j = \alpha I_{TE}/K$ of the TEG, and (d) the efficiency η of the hybrid system varying with variables V_{PV} and R_{L2}/R , where the values of the parameters are same as Fig. 2.

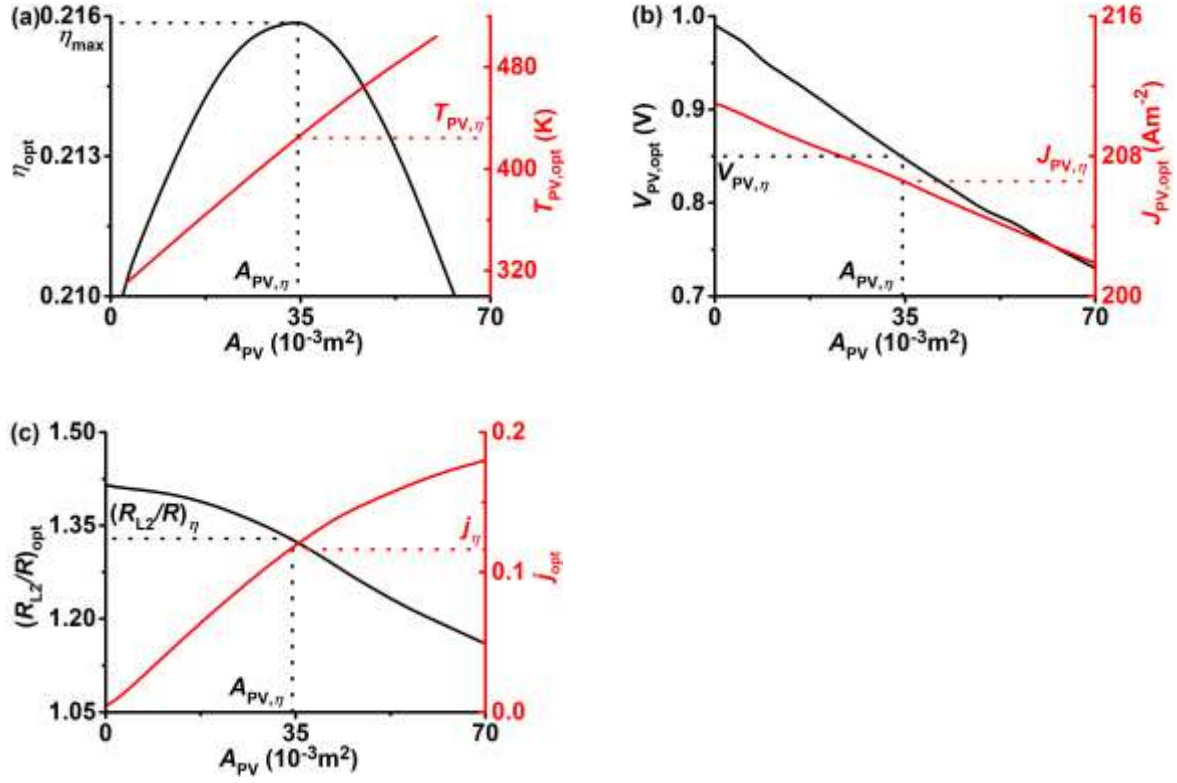


Fig. 6. (a) The optimal efficiency η_{opt} and PSC temperature $T_{PV,\text{opt}}$, (b) the optimal voltage $V_{PV,\text{opt}}$ and current density $J_{PV,\text{opt}}$ of the PSC, and (c) the optimal resistance ratio $(R_{L2}/R)_{\text{opt}}$ and dimensionless electric current j_{opt} of the TEG as a function of the area A_{PV} .

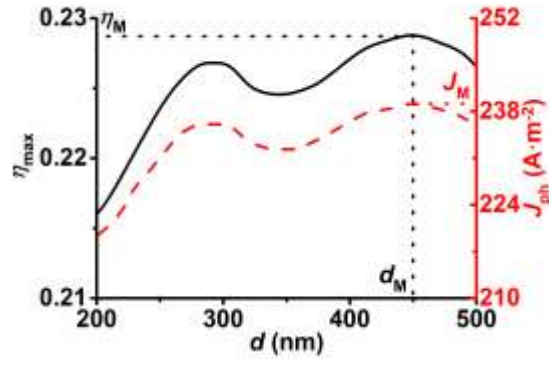


Fig. 7. The curves of the maximum efficiency η_{\max} and the photo-current density J_{ph} as a function of d .

Table 1. The performance comparisons between the present work and Refs. [10-13].

Research works	η_{\max}	$V_{\text{OC}}(\text{V})$	$J_{\text{SC}}(\text{Am}^{-2})$	$\Delta T(\text{K})$
Xu <i>et al.</i> [10]	13.4%	0.92	222	18
Fu <i>et al.</i> [11]	12.7%	6.67	30.6	10
Zhou <i>et al.</i> [12]	23.0%	1.26	251	8
Liu <i>et al.</i> [13]	12.6%	1.24	189	12
Present work	20.8%	1.40	219	19